S-Wave Attenuation Characteristics Beneath the Vrancea Region (Romania)–New Insights from the Inversion of Ground Motion Spectra

by

Adrien Oth[1,4], Dino Bindi[2], Stefano Parolai[3] and Friedemann Wenzel[4]

1) European Center for Geodynamics and Seismology, Luxembourg

2) Istituto Nazionale di Geofisica e Vulcanologia, Milan, Italy

3) GeoForschungsZentrum Potsdam, Germany

4) Geophysical Institute, University of Karlsruhe, Germany

Corresponding author: Adrien Oth
European Center for Geodynamics and Seismology
19, rue Josy Welter
L-7256 Walferdange
Luxembourg
Phone: +352 331487-35
Fax: +352 331487-88
Email: adrien.oth@ecgs.lu

ABSTRACT

The S-wave attenuation characteristics beneath the Vrancea region in Romania are analyzed from the spectra (frequency range 0.5-20 Hz) of more than 850 recordings at 43 accelerometric stations of 55 intermediate-depth earthquakes (M= 4.0-7.1) which occurred in the Vrancea seismogenic zone. The method commonly chosen for this type of investigation in the case of crustal earthquakes is the generalized inversion technique (GIT) (e.g. Andrews, 1986; Castro et al., 1990). Yet, the Vrancea dataset is entirely different from common crustal datasets. Due to the strong clustering of the hypocenters within a very small focal volume, there are only few crossing ray paths from sources to receivers. As a consequence, inhomogeneities in the attenuation properties are not averaged out, which leads to unphysical results if the standard GIT approach is adopted. The problem is discussed qualitatively by performing tests with synthetic data and solved quantitatively by adapting the GIT technique in view of these peculiarities. With the optimally adapted inversion scheme, it is possible to unravel differences in the attenuation characteristics between two (or more) sets of stations. The results show that the attenuation of seismic waves is roughly comparable in the low frequency range (< 4-5 Hz), but stronger by up to an order of magnitude at higher frequencies within the Carpathian mountain arc as compared with the foreland area. Modeling this strongly frequency-dependent lateral variation of seismic attenuation by a significantly lower Q beneath Vrancea (1) provides a very good fit of observed strong motion characteristics, (2) sheds new light on the distribution of intensities of the previous strong earthquakes, (3) will have strong implications for future hazard assessment, and (4) is fully compatible

with structural models from deep seismic sounding, tomography, and teleseismic attenuation.

INTRODUCTION

The high level of seismic hazard for Romania and especially for the city of Bucharest is almost entirely due to the intermediate-depth seismicity within the Vrancea seismogenic zone (e.g. Lungu et al., 1999; Sokolov et al., 2004). During the last century, four large Vrancea earthquakes with moment magnitudes higher than 6.5 occurred here. These earthquakes show the peculiarity that the hypocenters are clustered in a very narrow source volume. The epicentral area is limited to approximately 30×70 km^2 and the depth range extends from around 80 to 200 km (Figure 1). Furthermore, there is a seismic gap at 40-70 km depth separating the intermediate-depth from the less pronounced crustal seismicity (Fuchs et al., 1979).

Seismic attenuation (whose anelastic part is commonly characterized by the quality factor Q) and its frequency dependence can provide valuable information on the underground structure and are important quantities in view of seismic hazard assessment. In fact, they strongly influence the distribution of ground motion parameters and are needed for the simulation of realistic strong motion time histories, for instance when using the stochastic technique (e.g. Boore, 2003). Previous studies have been dealing with the spectral attenuation characteristics beneath Vrancea (Popa et al., 2005; Russo et al., 2005, Sudhaus and Ritter, 2005; Weidle et al., 2007) and their results will be discussed in conjunction with those of this study. However, no systematic analysis of the spectral attenuation characteristics over a large frequency band using a rigorous inversion procedure has been performed for the Vrancea area as yet, and the main purpose of this study is to fill this gap using the largest amount of accelerometric data available. The analyzed frequency range extends from 0.5 to 20 Hz.

For attenuation studies with datasets from crustal earthquakes, a commonly applied method is the generalized inversion technique (GIT) (Castro et al., 1990; Parolai et al., 2000, 2004; Bindi et al., 2006), which can be used to separate source, path (i.e. attenuation) and site effects contributing to the Fourier amplitude spectra of ground motion. In the case of Vrancea earthquakes, however, the geometry of the dataset is entirely different from the common crustal case. As the sources are all clustered in approximately the same location (Figure 1), there are few crossing ray paths between different source-station pairs and all rays from the different sources to a given station are almost identical. Whereas for usual datasets of crustal earthquakes, due to many ray crossings, differences in attenuation along different ray paths can be viewed to average out and the determination of an average attenuation curve with distance at each analyzed frequency makes sense, this is not the case for Vrancea earthquakes, as we show below. Furthermore, due to the depth range of these events, the lowest hypocentral distance in the dataset is about 90 km. These problems are inherent to the dataset and cannot be avoided in any study of seismic attenuation for the Vrancea case. However, we show in this article that with some modifications in the GIT inversion scheme, these difficulties can be overcome to a large extent. Hence this study contributes both to the further development of the GIT approach and provides new insights into the attenuation of seismic waves beneath Vrancea.

We first present results obtained by applying the standard GIT procedure to the dataset. Synthetic tests are carried out to show that the standard procedure is inefficient in providing reliable attenuation estimates when lateral variability is expected in the attenuation characteristics. After a modification of the GIT inversion scheme to account for this variability, the attenuation characteristics for two separate regions (within the Carpathian arc and around it) are derived in one common inversion.

DATABASE

We analyze seismograms from 52 earthquakes recorded by 43 stations (Figure 1) of the accelerometer network deployed in Romania since 1997 in the framework of the Collaborative Research Center (CRC) 461: 'Strong Earthquakes – A Challenge for Geosciences and Civil Engineering'. The stations consist of three-component accelerometers equipped with Kinemetrics K2-dataloggers with Global Positioning System (GPS) timing. Fifteen of the stations are deployed within the city limits of Bucharest, ten of which are used in this study (these stations are not all labeled on the map in Figure 1). The sampling rate of the data from this network is 200 samples/sec. The records were corrected for instrumental response and bandpass-filtered between 0.1 and 50 Hz using standard Kinemetrics software.

The magnitude range of the Vrancea earthquakes recorded with acceptable signal-to-noise ratio (SNR) with this network ranges from 4.0 to 5.8. This dataset was complemented with several strong motion recordings from the three large Vrancea earthquakes which occurred on August 30th, 1986 (M_W=7.1, eight records), May 30th, 1990 (M_W=6.9, eight records) and May 31st, 1990 (M_W=6.4, three records). These are analogue SMA-1 recordings obtained by a network operated by the National Institute for Earth Physics (NIEP) (Oncescu et al., 1999b). These data have been scanned and digitized at NIEP, the digitized recordings having a sampling rate of 100 samples/sec.

Thus, in total, more than 850 records from 55 Vrancea earthquakes recorded at 43 sites are used in this study. The hypocentral coordinates were extracted from the ROMPLUS catalogue (Oncescu et al., 1999a) and the depth range of the events (Figure 1) ranges from 70 to 180 km. An example for a three-component recording is shown in Figure 2. Due to the near-vertical incidence, the P-wave on the vertical (Z) component depicts large amplitudes, with maximum energy in the frequency range around 8-10 Hz.

Very little S-wave energy is seen on the Z component, and in many cases, it is entirely missing. At some stations located in the forearc region, such as GRE shown in Figure 2, strong high-frequency arrivals can occasionally be found on the Z component around 5 to 8 s before the S-wave arrival on the horizontal components. These may be related to S-P conversions at the base of the deep Focsani basin (with depths up to 22 km, Hauser et al., 2007). As a result of the missing S-wave energy, the Z component can of course not be used to derive S-wave attenuation properties. The observations mentioned above are however worth further investigations and have important consequences with respect to the estimation of site amplification effects using the H/V spectral ratio method, as we discuss elsewhere (Oth, 2007).

In the following, the S-wave portions of the horizontal component accelerograms are used. Time windows starting 1 s before the S-wave onset and ending when 80% of the total energy of the record are reached were extracted and tapered with a 5% cosine window. Typical window lengths range between 5 and 15 s. In the few cases where the determined window was longer than 20 s, it was fixed to a maximum duration of 20 s to avoid having too much code energy in the analyzed time windows. The Fourier amplitude spectra (FAS) were computed for each window and smoothed around 30 frequency points equidistant on logarithmic scale between 0.5 and 20 Hz using the windowing function proposed by Konno and Ohmachi (1998), with b = 20. Noise spectra were computed from pre-event noise windows of equal length as the considered signal windows, and at each of the chosen 30 frequencies, only data points with a SNR higher than three were included in the final dataset. Below 0.5 Hz, the SNR was generally not acceptable for the smaller earthquakes (mostly smaller than 1.5-2). As a result, the database is slightly sparser at the lowest frequencies. Finally, the root-mean-square (rms) average of the two horizontal component spectra was computed. Figure 3 shows several examples of the chosen time windows and the respective spectra.

METHODOLOGY AND SYNTHETIC DATA TESTS

The generalized inversion technique (GIT) (Andrews, 1986; Castro et al., 1990) is a well-studied method to derive frequency-dependent attenuation characteristics as well as source and site spectra, especially in the case of crustal earthquakes (e.g. Parolai et al., 2000, 2004; Bindi et al., 2006). There are essentially two ways to tackle the inversion: either a parametric approach is adopted (i.e. the attenuation along the travel path is assumed to follow a particular functional form, e.g. Salazar et al., 2007) and the inversion is performed in one step to obtain source and site spectra and a $Q(f)$-model, or attenuation is only constrained to be a smooth, decaying function with distance, which is the non-parametric approach introduced by Castro et al. (1990). With the parametric approach, it is a common problem that negative $Q(f)$-values are obtained. Such results can for instance be due to the assumptions regarding the geometrical spreading, as discussed by Castro et al. (1990), or to the simple fact that the seismic attenuation in a given region cannot be appropriately described with the commonly utilized, simple parameterizations.

Therefore, we follow the non-parametric approach, which splits the inversion into two steps: first, the dependence of the spectral amplitudes *U(f,r)* at frequency *f* on distance may be written as:

$$U_{ij}(f, r_{ij}) = A(f, r_{ij}) \cdot \hat{S}_j(f), \tag{1}$$

where $U_{ij}(f, r_{ij})$ is the spectral amplitude (acceleration) at the i-th station resulting from the j-th earthquake, r_{ij} is the source-site distance, $A(f, r_{ij})$ is the function describing seismic attenuation with distance and $\hat{S}_j(f)$ is a scaling factor depending on the size of the j-th event. $A(f, r_{ij})$ is not supposed to have any specific shape and implicitly contains all effects leading to attenuation along the travel path (geometrical spreading, anelasticity,

scattering …). Based on the idea that these properties vary slowly, $A(f, r_{ij})$ is constrained to be a smooth function of distance (i.e. with a small second derivative, Castro et al., 1990) and to take the value $A(f, r_0) = 1$ at some reference distance r_0.

The representation given by (1) does not include a factor related to the site, and hence, the site effects are necessarily absorbed both in $A(f, r_{ij})$ and $\hat{S}_j(f)$. $\hat{S}_j(f)$ contains in fact an average value of the site amplifications of all stations which recorded the j-th earthquake. Thus, $\hat{S}_j(f)$ is not the true source spectrum of the j-th event. The smoothness constraint mentioned above is implemented by a weighting factor (see e.g. Castro et al., 1990 and below) and is supposed to suppress rapid undulations in the attenuation function. This weighting factor must be reasonably chosen in order to suppress site-related effects and yet preserve variations of the attenuation characteristics with distance.

After the attenuation functions have been determined, a subsequent inversion allows separating source and site effects (Andrews, 1986):

$$R_{ij}(f) = S_j(f) \cdot Z_i(f) . \tag{2}$$

Herein, $R_{ij}(f) = U_{ij}(f, r_{ij}) / A(f, r_{ij})$ are the residual spectral amplitudes after correction of the attenuation functions, $S_j(f)$ is the source spectrum of the j-th earthquake and $Z_i(f)$ the site amplification function at station i. In this article, we focus on the attenuation characteristics $A(f, r_{ij})$ resulting from the first step, and the site amplification and source spectra obtained from the second inversion step are discussed elsewhere (Oth 2007).

Equation (1) can be easily linearized by taking the logarithm:

$$\log_{10} U_{ij}(f, r_{ij}) = \log_{10} A(f, r_{ij}) + \log_{10} \hat{S}_j(f) , \tag{3}$$

Equation (3) represents a linear system of the form $\mathbf{Ax} = \mathbf{b}$, where $\mathbf{b}$ is the data vector containing the logarithmic spectral amplitudes, $\mathbf{x}$ is the vector containing the model parameters and $\mathbf{A}$ is the system matrix relating the two of them. Practically, the distance range of the data (Figure 4) is divided into N_D bins, in our case 10 km wide, and the value of $A(f, r_{ij})$ is computed in each bin. In matrix formulation, equation (3) takes the form:

$$\left(\begin{array}{ccccc|ccccc} 1 & 0 & 0 & \cdot & \cdots & 1 & 0 & 0 & \cdot & \cdots \\ 0 & 1 & 0 & \cdot & \cdots & 1 & 0 & 0 & \cdot & \cdots \\ \cdot & \cdot & \cdot & \cdot & \cdots & \cdot & \cdot & \cdot & \cdot & \cdots \\ 1 & 0 & 0 & \cdot & \cdots & 0 & 1 & 0 & \cdot & \cdots \\ \vdots & \vdots & \vdots & \vdots & \vdots & \vdots & \vdots & \vdots & \vdots & \vdots \\ w_1 & 0 & 0 & \cdot & \cdots & \cdot & \cdot & \cdot & \cdot & \cdots \\ -w_2/2 & w_2 & -w_2/2 & \cdot & \cdots & \cdot & \cdot & \cdot & \cdot & \cdots \\ 0 & -w_2/2 & w_2 & -w_2/2 & \cdots & \cdot & \cdot & \cdot & \cdot & \cdots \\ \cdot & \cdot & \cdot & \cdot & \cdots & \cdot & \cdot & \cdot & \cdot & \cdots \end{array}\right) \cdot \left(\begin{array}{c} \log_{10} A_1 \\ \cdot \\ \cdot \\ \cdot \\ \log_{10} A_{N_D} \\ \log_{10} \hat{S}_1 \\ \cdot \\ \cdot \\ \log_{10} \hat{S}_{N_E} \end{array}\right) = \left(\begin{array}{c} \log_{10} U_{11} \\ \cdot \\ \cdot \\ \log_{10} U_{ij} \\ \vdots \\ 0 \\ 0 \\ 0 \\ \cdot \end{array}\right) \cdot \tag{4}$$

The weighting factor w_1 is used to impose $A(f, r_0) = 1$ at the reference distance and w_2 is the factor determining the degree of smoothness of the solution, as discussed above. The reference distance is set to 90 km, which is the smallest hypocentral distance in our dataset. This very large reference distance is problematic, since setting $A(f, r_0) = 1$ at r_0=90 km is in fact equal to assuming that there is no attenuation over that distance. Hence there is a cumulative attenuation effect over these 90 km which it is impossible to resolve in an absolute sense, but this cumulative effect plays a crucial role in the modification of the GIT scheme discussed further below in order to account for lateral variability of attenuation characteristics beneath Vrancea.

At each of the 30 selected frequencies, the least squares solution $\mathbf{x} = (\mathbf{A}^T\mathbf{A})^{-1}\mathbf{A}^T\mathbf{b}$ (if the system is numerically stable) can be computed by means of an appropriate inversion scheme (e.g. singular value decomposition, which we use in this work, Menke, 1989). In

order to assess the stability of the inversion results, we perform 200 bootstrap inversions (Efron and Tibshirani, 1994) at each frequency point following the procedure explained in Parolai et al. (2001, 2004). Given an original dataset of N_{rec} datapoints, this technique works by repeated inversions of datasets obtained by randomly resampling the original one. From the 200 bootstrap samples, the mean and standard error are calculated for each model parameter.

First results: failure of the standard approach

In a first attempt, we applied the standard non-parametric GIT to derive $A(f,r)$ as described above. The results at four selected frequencies are shown in Figure 5. At low frequencies (upper panel), the attenuation functions are more or less monotonically decaying, with a flat portion in the distance range 150-200 km. At frequencies higher than about 4-5 Hz, a bump starts to appear in this distance interval, the effect getting stronger and stronger with increasing frequency (bottom panel). Even though it is not unusual that an attenuation function flattens or even gets sloped upward in certain distance ranges due to e.g. critically reflected arrivals from the Moho in the case of crustal earthquakes (Bindi et al., 2006), both the shape and the amplitude of the bump in the attenuation functions at high frequencies obtained here are unphysical. For instance, the curve at a frequency of 15.51 Hz in Figure 5 does not show any decay, with values of $A(f,r)>1$ everywhere except at the largest hypocentral distances.

Visual inspection of the spectral amplitudes versus distance reveals that the stations MLR, SIR, VRI, PLO, GRE and OZU, all located directly within the Carpathian arc bending zone (VRI, PLO and SIR are covered by the stars marking the epicenters in Figures 1 and 6) or close to it, show systematically much lower amplitudes at high frequencies than the other stations of the network (Figure 7). The difference reaches about one order of magnitude for a given distance at frequencies higher than 8-10 Hz.

Therefore, these six stations are herein after regrouped into ‘region 2’, while the rest of the stations, almost all of them located in the forearc area, are regrouped in ‘region 1’ (Figure 6). With the introduction of these two regions, radial variations of ground motion (i.e. away from the epicenter) are taken into account, as region 2 is more or less restricted to the epicentral area. In order to also unravel azimuthal variations, a denser network with enough stations in all azimuth ranges around the epicenters would be required.

This remarkable difference in spectral amplitudes could in principle be explained either by a source, site or attenuation effect. Regarding the source, directivity is an improbable cause, as the effect also appears for small earthquakes, for which this source effect is rather unimportant due to the very small source size of the smaller Vrancea earthquakes and the considered distances (Oth et al., 2007). As the effect appears at high frequencies, the radiation pattern cannot lead to these systematic differences. If the radiation pattern were the cause, one should rather expect to see systematic differences more clearly at low frequencies, as the influence of the radiation pattern decreases with increasing frequency (e.g. Takenaka et al., 2003; Castro et al., 2006).

The possibility that these large differences in amplitude result from different site and basin effects is also unlikely, because except GRE, all the sites in region 2 are classified as rock stations. If site conditions were the cause, one would expect that a station such as SEC or FUL, located in the deep Focsani basin (Hauser et al., 2007), should show large amplification at some low resonance frequency (as the basin is very deep, see e.g. Bard, 1999) and large attenuation at high frequencies due to the strong damping in the sediments. However, the opposite of this expected effect is observed.

Hence, a strong difference of attenuation along the travel path is the preferred explanation for these results. In order to verify this hypothesis, we will now summarize the results of two synthetic data tests.

Synthetic data tests

The first test is intended to verify whether the bump is a simple problem related to the geometry of the dataset. Therefore, no inhomogeneities in attenuation are considered when generating the synthetic data, using a homogeneous halfspace Q-model (*model A*). With the second test, we investigate whether the bump observed before can be reproduced under the assumption of a variation of Q between region 1 and 2 (*model B*).

Both synthetic datasets have exactly the same number of stations and sources as well as the same geometry (i.e. source-station configuration) as the real data. The synthetic acceleration spectra are computed following the standard spectral model as used for stochastic point source simulations (Boore, 1983; 2003):

$$U(M_0, f, r) = (2\pi f)^2 C\, S(M_0, f)\, P(f, r)\, Z(f) \tag{5}$$

with

$$C = \frac{\Re^{\theta\varphi} V F}{4\pi\rho\, v_S^3 r_0} \text{ and } P(f, r) = \frac{1}{r}\exp\left(-\frac{\pi f r}{Q(f) v_S}\right). \tag{6}$$

In equation (5), $U(M_0, f, r)$ denotes the acceleration spectrum, $S(M_0, f)$ the source spectrum, $P(f, r)$ the propagation path effect (i.e. equivalent to $A(f, r)$) and $Z(f)$ the site amplification function. Furthermore, M_0 is the seismic moment, r the hypocentral distance, $\Re^{\theta\varphi} = 0.6$ the average S-wave radiation pattern, $F = 2$ the free surface amplification, $V = 1/\sqrt{2}$ accounts for the splitting of shear wave energy into two horizontal components. $\rho = 3.2\ \mathrm{g/cm^3}$ is the density and the average shear wave velocity is set to $v_S = 4.5\ \mathrm{km/s}$, which is an acceptable approximation following the seismic tomography results of Martin et al. (2006).

The two $Q(f)$-models used are listed in Table 1. For *model A*, a homogeneous halfspace is assumed, whereas for *model B*, attenuation along travel paths to stations in

region 2 is stronger (i.e. Q is lower) than along paths ending in region 1. The frequency dependence is chosen such that the difference in attenuation increases with increasing frequency, in agreement with the observations regarding the spectral amplitudes. These $Q(f)$-models are arbitrarily chosen, but close to models used by other authors (e.g. Sokolov et al., 2005). Since the purpose of these synthetic tests is only to show that lateral variations of the frequency-dependent attenuation characteristics can indeed explain the shape of the attenuation functions, but not to derive quantitative results from them (this is done by modification of the original inversion scheme further below), this degree of arbitrariness is justified.

The source spectra are modeled following the classical Brune (1970, 1971) model:

$$S(M_0, f) = M_0 \left[1 + \frac{f^2}{f_C^2} \right]^{-1}, \tag{7}$$

where f_c is the corner frequency of the spectrum. The corner frequencies of the synthetic events are randomly chosen, yet decreasing with increasing magnitude. For different magnitude bins, the bounds inbetween which f_c is chosen randomly are different. For instance, f_c is given in the interval 5-10 Hz for $4 \leq M_W < 4.5$ and 2-6 Hz for $4.5 \leq M_W < 5$. The ranges are deliberately chosen this high, as high corner frequencies are expected for Vrancea earthquakes (Oncescu, 1989; Oth et al., 2007).

For each of the two $Q(f)$-models, site effects in equation (5) were once modeled using the H/V ratios (Lermo and Chávez-García, 1993) and once simply neglected in order to assess the influence of site amplification on the shape of the resulting attenuation curves. Here we show the results obtained including the site effect estimate, but the bump in the attenuation curves discussed below proved to be a stable feature, no matter if an estimate of site amplification is included in the synthetic spectra or not. Finally, normally

distributed random noise with a standard deviation of 10% of the respective data values is added to the synthetic spectra.

The resulting attenuation curves $A(f,r)$ are shown for two frequencies in Figure 8 a) and b) for *model A* and *B*, respectively. For *model A*, the attenuation functions are also monotonically decaying at high frequencies, which clearly shows that the spurious results obtained with the real dataset are not related to the geometry of the dataset. Apart from slight deviations from the theoretical model (related to the assumed site effects, as these deviations are not present when the site effect free synthetics are used) at few frequencies, the attenuation model can be acceptably well reproduced by the inverted solution. The attenuation functions obtained using the attenuation *model B*, however, depict a striking similarity with the results shown in Figure 5. Instead of obtaining attenuation functions in between the two attenuation models for region 1 and 2, a strong bump is obtained. This outcome strongly suggests that the variation in spectral amplitudes between region 1 and 2 is the result of inhomogeneities in whole path attenuation not correctly taken into account by the standard GIT procedure. From the histograms of the distribution of data points with hypocentral distance shown in Figure 9, one can see that the stations in region 2 have a strong influence at smaller hypocentral distances, with a maximum number of data around 150 km. With increasing distance, their influence is constantly reduced until they disappear for distances higher than 180 km. Since, at high frequencies, the spectral amplitudes are much larger in region 1 even for large distances (see Figure 7, lower panel) as compared with those in region 2, the bump in the attenuation functions is unavoidable if a single attenuation function is fit to the data at each frequency point.

In order to account for lateral variability in the attenuation characteristics between the two regions, the inversion scheme presented in equations (3) and (4) is adapted to this

new situation and separate attenuation functions for the two regions are derived in a single inversion.

The adapted inversion scheme

The adapted inversion scheme can be written as:

$$\log_{10} U_{ij}(f, r_{ij}) = p_1 \cdot \log_{10} A_1(f, r_{ij}) + p_2 \cdot \log_{10} A_2(f, r_{ij}) + \log_{10} \hat{S}_j(f), \qquad (8)$$

where p_1 equals one if the considered station is located in region 1 and otherwise zero and p_2 is defined the opposite way. $A_1(f, r)$ is discretized into N_{D1} while $A_2(f, r)$ is discretized into N_{D2} equally sized bins (10 km in both regions), with $N_{D2} < N_{D1}$ in the case analyzed here (as the maximum hypocentral distance for region 2 is approximately 180 km). For both attenuation functions, the reference distance is set to r_0=90 km. Regarding the constraints, we impose $A_1(f, r_0) = 1$ whereas the origin (i.e. the value of $A_2(f, r_0)$) of $A_2(f, r)$ is free. These constraints allow accounting for the fact that not only the decay with distance, but also the general level of the spectral amplitudes may be different between the two cases, which, as shown above, is clearly the case for Vrancea earthquakes. In other words: the shift of the origin between the two attenuation functions reflects the (cumulative) difference in attenuation over the distance r_0 for both sets of travel paths defined by regions 1 and 2. Both attenuation functions are of course also constrained to be smooth functions of distance.

The system matrix **A** as given in equation (4) then takes the following form:

$$\left(\begin{array}{ccccc|ccccc|cccc}
1 & 0 & 0 & \cdot & \cdots & 0 & 0 & 0 & \cdot & \cdots & 1 & 0 & 0 & \cdots \\
0 & 0 & 0 & \cdot & \cdots & 1 & 0 & 0 & \cdot & \cdots & 1 & 0 & 0 & \cdots \\
\cdot & \cdot & \cdot & \cdot & \cdots & \cdot & \cdot & \cdot & \cdot & \cdots & \cdot & \cdot & \cdot & \cdots \\
0 & 1 & 0 & \cdot & \cdots & 0 & 0 & 0 & \cdot & \cdots & 0 & 1 & 0 & \cdots \\
\vdots & \vdots & \vdots & \vdots & \vdots & \vdots & \vdots & \vdots & \vdots & \vdots & \vdots & \vdots & \vdots & \vdots \\
w_1 & 0 & 0 & \cdot & \cdots & 0 & 0 & 0 & \cdot & \cdots & \cdot & \cdot & \cdot & \cdots \\
-w_2/2 & w_2 & -w_2/2 & 0 & \cdots & 0 & 0 & 0 & \cdot & \cdots & \cdot & \cdot & \cdot & \cdots \\
0 & -w_2/2 & w_2 & -w_2/2 & \cdots & 0 & 0 & 0 & \cdot & \cdots & \cdot & \cdot & \cdot & \cdots \\
\cdot & \cdot & \cdot & \cdot & \cdots & \cdot & \cdot & \cdot & \cdot & \cdots & \cdot & \cdot & \cdot & \cdots \\
0 & 0 & 0 & 0 & \cdots & -w_2/2 & w_2 & -w_2/2 & 0 & \cdots & \cdot & \cdot & \cdot & \cdots \\
0 & 0 & 0 & 0 & \cdots & 0 & -w_2/2 & w_2 & -w_2/2 & \cdots & \cdot & \cdot & \cdot & \cdots \\
\cdot & \cdot & \cdot & \cdot & \cdots & \cdot & \cdot & \cdot & \cdot & \cdots & \cdot & \cdot & \cdot & \cdots
\end{array}\right), \tag{9}$$

and the new solution vector contains model parameters for both attenuation functions:

$$\mathbf{x}^T = \left(\log_{10} A_{1,1} \quad \ldots \quad \log_{10} A_{1,N_{D1}} \;\middle|\; \log_{10} A_{1,1} \quad \ldots \quad \log_{10} A_{1,N_{D2}} \;\middle|\; \log_{10} \hat{S}_1 \quad \ldots \quad \log_{10} \hat{S}_{N_E}\right)^T . \tag{10}$$

As for the original scheme, the source scaling factors $\log_{10} \hat{S}_j(f)$ include in this case the (logarithmic) average of the site amplification of the stations in region 1 which recorded the event, as the origin of $A_1(f,r)$ is fixed. Suppose that all earthquakes are recorded by all stations in region 1 and all stations in region 2 (which is of course not the case in reality). If now the average site amplification of the stations in region 1 differs from the one in region 2, this difference is also mapped into the offset of the two attenuation functions. However, as each event is recorded by a different combination of stations in region 1 and in region 2, the relation of the average site amplifications between the two regions is different for each earthquake, and thus, the effect will most likely average out. Therefore, it is a reasonable assumption to suppose that the shift of the origin of $A_2(f,r)$ relative to $A_1(f,r)$ is really entirely determined by the difference in attenuation along the paths.

RESULTS AND DISCUSSION

The attenuation functions resulting from the application of the modified scheme to the real data are shown for four selected frequencies in Figure 10. At low frequencies (upper panels), the origin of $A_2(f,r)$ is almost identical to the one of $A_1(f,r)$ (the latter one being constrained) and the slope of $A_2(f,r)$ is slightly larger. As the frequency increases (bottom panels), the origin of $A_2(f,r)$ is progressively shifted downward, with a maximum difference of about one order of magnitude at 15.51 Hz. The slopes of the functions are however very similar.

Note that both attenuation functions are now monotonically decaying, in contrast to the results obtained by fitting a single attenuation function to the entire dataset (Figure 5). For each of the two attenuation functions, $Q(f)$ can be evaluated by fitting a parametric model to $A(f,r)$:

$$A(f,r) = G(r)\exp\left(-\frac{\pi f r}{Q(f)v_S}\right), \tag{11}$$

where $G(r)$ is the geometrical spreading function. Due to the large depth of Vrancea earthquakes, surface waves are expected to play only a minor role in the geometrical spreading term. Therefore, the geometrical spreading function is chosen as $G(r) = r_0/r$, with r_0 being the reference distance of 90 km. Taking the logarithm of (11) and rearranging leads to:

$$\log_{10} A(f,r) - \log_{10} G(r) = -\frac{\pi f}{2.3Q(f)v_S} r\,. \tag{12}$$

The factor 2.3 in the denominator comes from $\log_{10}(e)$, which does not appear if the natural logarithm is used. Thus, by correcting the attenuation functions for geometrical

spreading and plotting versus distance, $Q(f)$ can be evaluated from the slope of a linear least squares fit. An example for this procedure is shown in Figure 11 (top).

With this procedure, however, only the slope of the attenuation function can be accounted for. Therefore, before fitting equation (12) to $A_2(f,r)$, we normalize $A_2(f,r)$ to equal 1 at $r=r_0$. The offset between the origins of the two functions (i.e. the difference between $A_1(f,r_0)$ and $A_2(f,r_0)$) corresponds to a cumulative difference in attenuation over r_0=90 km.

After $Q(f)$ has been determined at all 30 frequencies for both regions, we fit a model of the form $Q(f)=Q_0 f^N$ to the determined values (Figure 11, bottom) and obtain:

$$\begin{aligned} Q(f) &= 114 f^{0.96} \text{ for region 1} \\ Q(f) &= \ 72 f^{1.12} \text{ for region 2} \end{aligned} . \qquad (13)$$

Hence, $Q(f)$ follows a roughly linear trend with frequency in both regions. Surprisingly at first sight, these two $Q(f)$-models are almost identical. Remember however that these models are derived from the slope of the attenuation functions alone, not including the offset at the reference distance. A physical interpretation for this offset is provided further below.

Several other researchers already focused their attention on the seismic attenuation in the Carpathians and surroundings. Based on a qualitative discussion of a small set of seismograms, Popa et al. (2005) presented indications that strong lateral variability of upper-mantle attenuation characteristics must exist in order to be able to explain the large amplitude differences within the Carpathians and the foreland at frequencies higher than 1 Hz. Russo et al. (2005), with data from the same network as used here, computed the ratios between the spectra of S and P waves to derive differential Q_S estimates. They obtained average Q_S values around 100-250 for stations within the Carpathian arc and up

to 1000 for stations in the foreland, reaching thus similar conclusions as Popa et al. (2005). Their analysis technique, however, makes strong assumptions both regarding the source (identical source spectra for P- and S-waves) and site (equality of site amplification on the horizontal component of S- and vertical component of P-waves) contributions to the ground motion spectra. Sudhaus and Ritter (2005) and Weidle et al. (2007) used teleseismic data to derive t* measurements at low frequencies (< 1-1.5 Hz) and also found significant lateral variations of attenuation.

In general, the results of the above-mentioned studies are in good agreement with those presented in this article. This study represents the first systematic analysis of the frequency dependence of seismic attenuation beneath Vrancea and its lateral variations. At low frequencies, the difference between the two regions is not extremely striking in our study. There is no offset between the origins of the two attenuation functions and the slope of the function in region 2 is somewhat larger. This observation is consistent with the results of Weidle et al. (2007), who found the largest t* values (i.e. the largest attenuation) at stations located in the epicentral zone of Vrancea earthquakes. At high frequencies, the variation in attenuation between region 1 and 2 becomes larger and larger, quantified through the offset of the attenuation functions origins. The slopes of the functions, however, are quite similar, leading to the determination of roughly identical $Q(f)$-models.

An attempt to explain this observation is illustrated in Figure 12. As can be seen from the distribution of the earthquake hypocenters (Figure 1), they are all located approximately directly beneath the stations in region 2. Thus, in order to increase the distance in $A_2(f,r)$, the source depth has to be increased. The difference in travel path for two data points at different distances in region 2 are hence related to the path traveled from the deeper event's hypocenter up to the one of the shallower one. As schematically

indicated in Figure 12, within the grayshaded area, all the rays travel more or less the same path. In conclusion, $A_2(f,r)$ only 'samples' the lower part of the travel path, whereas the large offset observed between $A_1(f,r_0)$ and $A_2(f,r_0)$ is related to some strongly attenuating region somewhere in the grayshaded area, approximately between the shallowest event's hypocenter and the surface.

The seismic tomography results presented by Martin et al. (2006) and the outcome of the seismic refraction studies (Hauser et al., 2001, 2007) provide indications on the reasons for these strong lateral variations in seismic attenuation. The seismic refraction data (Hauser et al., 2001) suggest the presence of a low-velocity zone at a depth of 47 to 55 km beneath the Vrancea region, which, as Sperner et al. (2005) note, coincides quite well with the observed seismic gap between 40 and 70 km depth already discussed by Fuchs et al. (1979). Here, the slab seems to be mechanically decoupled (or only weakly coupled) from the crust through a weak zone. This zone is commonly interpreted as the place where slab detachment currently takes place. This area of weak coupling could be an explanation for the lower spectral amplitudes in the vicinity of the epicentral area (region 2) and the offset between the attenuation functions for the two regions. Russo et al. (2005) invoke the existence of thermal anomalies influencing the travel paths to the stations SIR and MLR in view of recent volcanism at several sites near these stations. Ismail-Zadeh et al. (2005), following the work of Demetrescu and Andreescu (1994), show that indeed very high temperatures might persist in the subcrustal mantle (at a depth of around 50 km) beneath the mountain arc.

Beneath the Transylvanian basin (i.e. behind the mountain arc), the tomography (Martin et al., 2006) clearly reveals a very strong low-velocity anomaly in the depth range 35-110 km, which is interpreted as the result of slab rollback and the delamination of continental lithosphere. Additionally, Martin et al. (2006) invoke the possible presence of

partial melts at depth of approximately 100 km. The strong contrast between the high-velocity body (i.e. the slab with low attenuation), which influences the waves traveling to stations in the foreland (see tomography results, Martin et al., 2006), and the very strong low-velocity anomaly behind the mountain range is proposed by Popa et al. (2005) to explain the observed variations in attenuation, especially in the Transylvanian basin. We can neither confirm nor reject this interpretation regarding sites behind the mountain arc with this data set, as no such location is included in the database studied (station OZU is the only site which is close to the Transylvanian basin, although still in the mountain arc).

Yet, an interesting observation in that direction is the fact that no single recording from stations DRG (46.79° N, 22.71° E) and MED (46.14° N, 24.37° E), located farthest to the NW from the Vrancea region (thus far behind the mountain arc), was usable for this analysis, hinting for strong signal attenuation. Although for smaller events the installation at noisy sites and the large hypocentral distances might provide an explanation for this evidence, they cannot provide a convincing explanation when also for the strongest events no clear S-wave signal can be detected. For instance, the recordings at DRG and MED (due to their very low amplitudes, these two stations would have been classified into region 2 if they would have been usable for the analysis) of the 2004/10/27 (M_W = 5.8) event show a clear P-onset, but no S-wave is detectable, neither on the horizontal nor on the vertical components, and the maximum amplitude is approximately 0.2 cm/s^2 (hypocentral distance ≈ 340 km) for DRG and 2.5 cm/s^2 for MED (hypocentral distance ≈ 215 km). At station ZIM (in region 1, at hypocentral distance ≈ 280 km), the S-wave is very clear, with a maximum amplitude of around 30 cm/s^2, which is more than one order of magnitude larger than at MED (which is even at closer distance to the source) and more than two orders of magnitude larger than at DRG. A very strong attenuation for travel paths behind the mountain arc might explain this peculiarity. Thus, the observed

inhomogeneity in attenuation is rather explainable by strong upper-mantle heterogeneity than crustal features. These variations in seismic attenuation between the foreland (region 1) on one hand and the mountain range (region 2) and backarc area on the other also have important implications for the seismic hazard of Romania. As Popa et al. (2005) also note, the difference in attenuation is most relevant at high frequencies. This view is clearly confirmed by this study with a much larger dataset, and the main advantage of the results presented here is that the variation in attenuation has been quantitatively analyzed by means of an inversion scheme. At low frequencies, the spectral amplitudes of ground motion have similar values in region 1 and 2. Thus, for structures sensitive to low frequencies, such as high-rise buildings or long-span bridges, the risk is similar in the mountain range (and behind) and in the foreland, depending of course on the distance from the source region. At high frequencies, this situation changes drastically. Within and behind the mountain arc, the risk for e.g. buildings with roughly less than three floors seems to be much smaller as compared with the foreland, as the high-frequency energy is efficiently attenuated for the latter region.

In view of the intensity maps from Vrancea earthquakes (the intensity maps of the large 1977 and 1986 events are shown in Oth et al., 2007, Figure 7), the observed variations in attenuation might be the key to understand the overall shape of the isoseismals. Apart from the small-scale structure within the high intensity (VII and VIII) areas (which are discussed in terms of source physics in Oth et al., 2007), it is striking that the isoseismals separating the high and low intensities almost exactly follow the shape of the mountain arc. Within the Carpathians as well as behind them, there are only few buildings sensitive to low frequencies (as Popa et al., 2005, note, the largest amount of tall buildings is found in Bucharest) and the structures sensitive to higher frequencies are less affected due to the strong attenuation of high-frequency seismic waves. Thus, the overall shape of the macroseismic intensity pattern can be explained by the combination of a less

endangered inventory of buildings (with respect to low frequencies) and strong attenuation of high-frequency energy within and behind the mountain arc as compared with the foreland.

It should be emphasized that the attenuation functions $A(f,r)$ contain all effects leading to seismic wave attenuation and that we cannot distinguish between the contributions of anelastic and scattering attenuation. As Furumura and Kennett (2005) show, internal heterogeneities within the subducted plate and particularly their shape play an important role in guiding high-frequency seismic signals. Weidle et al. (2007) show from anelastic attenuation modeling that it is not possible to explain their t*-observations from teleseismic earthquakes solely by anelasticity mechanisms. An especially strong indication for the influence of scattering effects in the attenuation of seismic waves is its strong frequency dependence (Furumura and Kennett, 2005). However, we cannot definitely conclude on these issues and further investigations are required in order to clarify the role of scattering attenuation as compared with intrinsic attenuation.

CONCLUSIONS

Seismic attenuation in the Carpathians and the surrounding areas depicts strong lateral variations, with very strong attenuation in the epicentral area (and, based on the findings of other authors mentioned above, probably also behind the mountain arc in the Transylvanian basin) and much lower attenuation in the foreland. Moreover, the variability strongly increases with increasing frequency. From synthetic data tests, we were able to show that the shape of the attenuation functions obtained applying the standard GIT approach can be well explained by such lateral, frequency-dependent variability of attenuation characteristics between the bending zone of the Carpathian arc and the foreland.

With a modification of the inversion scheme, it is possible to simultaneously invert for the attenuation properties of two (or more) regions in one single inversion, allowing us to quantify the lateral inhomogeneity at each analyzed frequency. At high frequencies (> 4-5 Hz), there is approximately one order of magnitude difference in attenuation between the mountain range and the foreland, whereas at lower frequencies, the attenuation characteristics are rather similar. Possible physical explanations for these results involve the degree of coupling between the slab and the overlying crust (Sperner et al. 2005), strong temperature variations (Ismail-Zadeh et al., 2005) as well as scattering phenomena within the subducted lithosphere (Furumura and Kennett, 2005).

Previous attempts of hazard assessment focussed on the azimuthal dependence of ground motion (Lungu et al., 1999; Sokolov et al., 2004). This study demonstrates that the radial variation is equally important: It allows to understand the intensity distribution of previous strong earthquakes and should be incorporated in future hazard assessment.

ACKNOWLEDGMENTS

This study was carried out in the Collaborative Research Center (CRC) 461 ‘Strong Earthquakes: a Challenge for Geosciences and Civil Engineering’, which is funded by the Deutsche Forschungsgemeinschaft (German Research Foundation) and supported by the state of Baden-Württemberg and the University of Karlsruhe. The ROMPLUS catalogue (Oncescu et al., 1999a) used in this study is continuously updated as new earthquakes occur and is available at http://www.infp.ro/catal.php.

REFERENCES

Andrews, D. J. (1986). Objective determination of source parameters and similarity of earthquakes of different size. In Das, S., Boatwright, J., and Scholz, C. H., editors, *Earthquake Source Mechanics*. American Geophysical Monograph 37, 259-267.

Bard, P.-Y. (1999). Local effects of strong ground motion: Physical basis and estimation methods in view of microzonation studies. In *Proceedings of the Advanced Study Course Seismotectonics and Microzonation Techniques in Earthquake Engineering: Integrated Training in Earthquake Risk Reduction Practices*. Kefallinia.

Bindi, D., Parolai, S., Grosser, H., Milkereit, C., and Karakisa, S. (2006). Crustal attenuation characteristics in Northwestern Turkey in the range from 1 to 10 Hz. *Bull Seismol. Soc. Am.*, 96:200–214.

Boore, D. M. (1983). Stochastic simulation of high-frequency ground motions based on seismological models of the radiated spectra. *Bull. Seismol. Sol. Am.*, 73:1865–1894.

Boore, D. M. (2003). Simulation of ground motion using the stochastic method. *Pure Appl. Geophys.*, 160:635–676.

Brune, J. N. (1970). Tectonic stress and the spectra of seismic shear waves from earthquakes. *J. Geophys. Res.*, 75:4997–5009.

Brune, J. N. (1971). Correction. *J. Geophys. Res.*, 76:5002.

Castro, R. R., Anderson, J. G., and Singh, S. K. (1990). Site response, attenuation and source spectra of S waves along the Guerrero, Mexico, subduction zone. *Bull. Seismol. Soc. Am.*, 80:1481–1503.

Castro, R. R., Franceschina, G., Pacor, F., Bindi, D., and Luzi, L. (2006). Analysis of the frequency dependence of the S-wave radiation pattern from local earthquakes in central Italy. *Bull. Seismol. Soc. Am.*, 96:415–426.

Demetrescu, C. and Andreescu, M. (1994). On the thermal regime of some tectonic units in a continental collision environment in Romania. *Tectonophysics*, 230:265–276.

Efron, B. and Tibshirani, R. J. (1994). *An Introduction to the Bootstrap*. Chapman & Hall, CRC.

Fuchs, K., Bonjer, K.-P., Bock, G., Cornea, I., Radu, C., Enescu, D., Jianu, D., Nourescu, A.,Merkler, G., Moldoveanu, T., and Tudorache, G. (1979). The Romanian

earthquake of March 4, 1977: II. Aftershocks and migration of seismic activity. *Tectonophysics*, 53:225–247.

Furumura, T. and Kennett, B. L. N. (2005). Subduction zone guided waves and the heterogeneity structure of the subducted plate: Intensity anomalies in Northern Japan. *J. Geophys. Res.*, 110, B10302, doi:10.1029/2004JB003486.

Hauser, F., Raileanu, V., Fielitz, W., Bala, A., Prodehl, C., Polonic, G., and Schulze, A. (2001). VRANCEA99 — The crustal stucture beneath the SouthEastern Carpathians and the Moesian Platform from seismic refraction profile in Romania. *Tectonophysics*, 340:233–256.

Hauser, F., Raileanu, V., Fielitz, W., Dinu, C., Landes, M., Bala, A., and Prodehl, C. (2007). Seismic crustal structure between the Transylvanian basin and the Black Sea, Romania. *Tectonophysics*, 430:1–25.

Ismail-Zadeh, A., Müller, B., and Schubert, G. (2005). Three-dimensional numerical modeling of contemporary mantle flow and tectonic stress beneath earthquake-prone SouthEastern Carpathians based on integrated analysis of seismic, heat flow and gravity data. *Phys. Earth Planet. Int.*, 149:81–98.

Konno, K. and Ohmachi, T. (1998). Ground-motion characteristics estimated from spectral ratio between horizontal and vertical components of microtremor. *Bull. Seismol. Soc. Am.*, 88:228–241.

Lermo, J. and Chávez-García, F. J. (1993). Site effect evaluation using spectral ratios with only one station. *Bull. Seismol. Soc. Am.*, 83:1574–1594.

Lungu, D., T. Cornea and C. Nedelcu (1999). Hazard assessment and site-dependent response for Vrancea earthquakes, in *Vrancea earthquakes: tectonics, hazard and risk mitigation*, F. Wenzel, D. Lungu and O. Novak, Editors, Kluwer Academic Publishers, Dordrecht, Netherlands, 251-268.

Martin, M.,Wenzel, F., and the CALIXTO working group (2006). High-resolution teleseismic body wave tomography beneath SE-Romania (II): Imaging of a slab detachment scenario. *Geophys. J. Int.*, 164:579–595.

Menke, W. (1989). *Geophysical Data Analysis: Discrete Inverse Theory*. International Geophysics Series, Academic Press.

Oncescu, M. C. (1989). Investigation of a high stress drop earthquake on August 30, 1986 in the Vrancea region. *Tectonophysics*, 163:35–43.

Oncescu, M. C., V. I. Marza, M. Rizescu and M. Popa (1999a). The Romanian earthquake catalogue between 984-1997, in *Vrancea earthquakes: tectonics, hazard and risk*

mitigation, F. Wenzel, D. Lungu and O. Novak, Editors, Kluwer Academic Publishers, Dordrecht, Netherlands, 43-48.

Oncescu, M. C., K.-P. Bonjer and M. Rizescu (1999b). Weak and strong ground motion of intermediate depth earthquakes from the Vrancea region, in *Vrancea earthquakes: tectonics, hazard and risk mitigation*, F. Wenzel, D. Lungu and O. Novak, Editors, Kluwer Academic Publishers, Dordrecht, Netherlands, 27-42.

Oth, A. (2007). *Source Processes and Spectral Ground Motion Models of Intermediate-Depth Vrancea (Romania) Earthquakes*. Ph.D. thesis, 189 pp., University of Karlsruhe, Germany.

Oth, A., Wenzel, F., and Radulian, M. (2007). Source parameters of intermediate-depth Vrancea (Romania) earthquakes from empirical Green's functions modeling. *Tectonophysics*, 438:33–56.

Parolai, S., Bindi, D., and Augliera, P. (2000). Application of the generalized inversion technique (GIT) to a microzonation study: numerical simulations and comparison with different site-estimation techniques. *Bull. Seismol. Soc. Am.*, 90:286–297.

Parolai, S., Bindi, D., Baumbach, M., Grosser, H., Milkereit, C., Karakisa, S., and Zünbül, S. (2004). Comparison of different site response estimation techniques using aftershocks of the 1999 Izmit earthquake. *Bull. Seismol. Soc. Am.*, 94:1096–1108.

Popa, M., Radulian, M., Grecu, B., Popescu, E., and Placinta, A. O. (2005). Attenuation in South-Eastern Carpathians area: result of upper mantle inhomogeneity. *Tectonophysics*, 410:235–249.

Russo, R. M., Mocanu, V., Radulian, M., Popa, M., and Bonjer, K.-P. (2005). Seismic attenuation in the Carpathian bend zone and surroundings. *Earth Planet. Sci. Lett.*, 237:695–709.

Salazar, W., Sardina, V., and de Cortina, J. (2007). A Hybrid inversion technique for the evaluation of source, path and site effects employing S-Wave spectra for subduction and upper-crustal earthquakes in El Salvador. *Bull. Seismol. Soc. Am.*, 97:208–221.

Sokolov, V. Yu., K.-P. Bonjer and F. Wenzel (2004). Accounting for site effects in probabilistic assessment of seismic hazard for Romania and Bucharest: a case of deep seismicity in Vrancea zone. *Soil Dynamics and Earthquake Engineering*, 24, 929-947.

Sokolov, V., Bonjer, K.-P., Onescu, M., and Rizescu, M. (2005). Hard rock spectral models for intermediate depth Vrancea (Romania) earthquakes. *Bull. Seismol. Soc. Am.*, 95:1749–1765.

Sperner, B. and the CRC 461 Team (2005). Monitoring of slab detachment in the Carpathians. In Wenzel, F., editor, *Perspectives in Modern Seismology*. Lecture Notes in Earth Sciences, Vol. 105, Springer Verlag, Berlin.

Sudhaus, H. and J. R. R. Ritter (2005). High-resolution measurement of the seismic attenuation across the Vrancea region, Romania. *Geophy. Res. Lett.*, Vol. 32, L10301, doi.: 10.1029/2004GL022148.

Takenaka, H., Mamada, Y., and Futamure, H. (2003). Near-source effect on radiation pattern of high-frequency S waves: Strong SH-SV mixing observed from aftershocks of the 1997 Northwestern Kagoshima, Japan earthquakes. *Phys. Earth Planet. Int.*, 137:31–43.

Weidle, C., F. Wenzel and A. Ismail-Zadeh (2007). t* - an unsuitable parameter to characterize anelastic attenuation in the Eastern Carpathians. *Geophs. J. Int.*, 170, 1139-1150.

Table 1. Q-models used in the synthetic data tests. Model A assumes a homogeneous halfspace, while in model B, seismic attenuation is stronger (i.e. Q is lower) in region 2 than in region 1, the difference between the two regions getting larger with increasing frequency (i.e. different frequency dependence).

model A	$Q_A(f) = 100 f^{0.8}$	
model B	Region 1	Region 2
	$Q_{B,1}(f) = 150 f^{0.8}$	$Q_{B,2}(f) = 100 f^{0.5}$

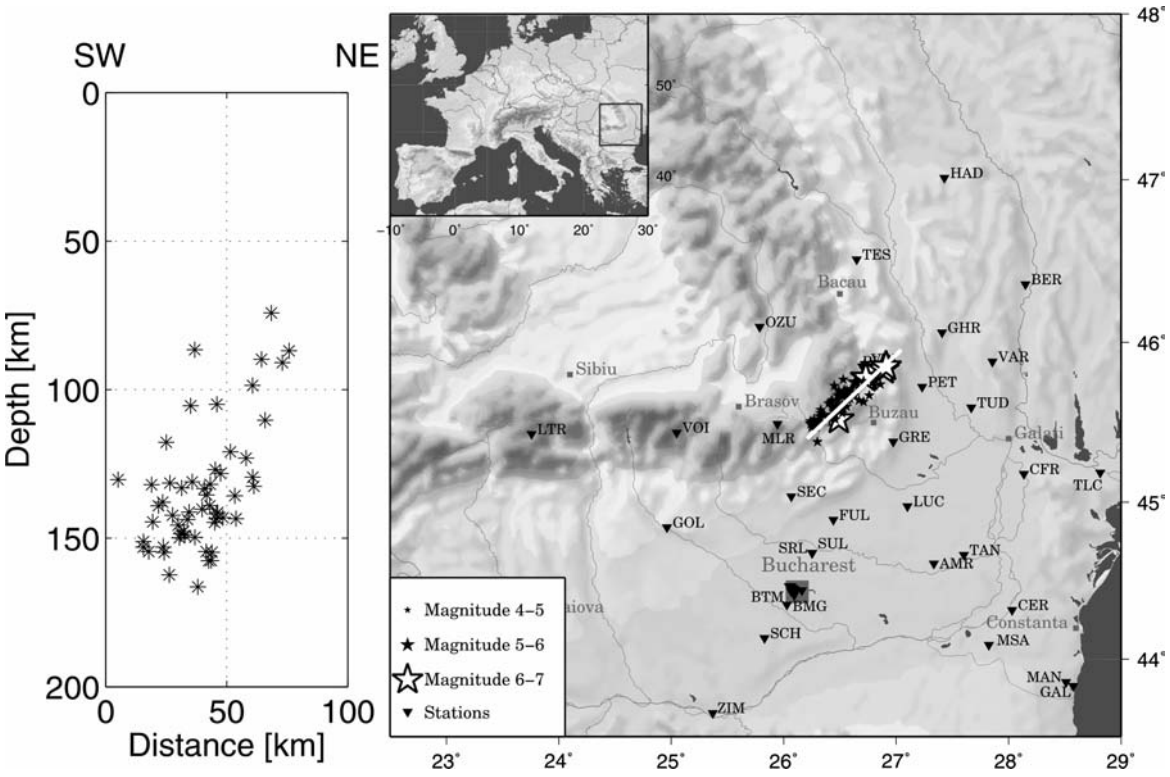

Figure 1. Map of Romania and source-station configuration. The epicenters of the utilized earthquakes are depicted by stars and the stations by inverse triangles. In total, 55 earthquakes and 43 stations have been used. On the left, a SW-NE vertical cross section through the epicentral area is shown (white line on the map).

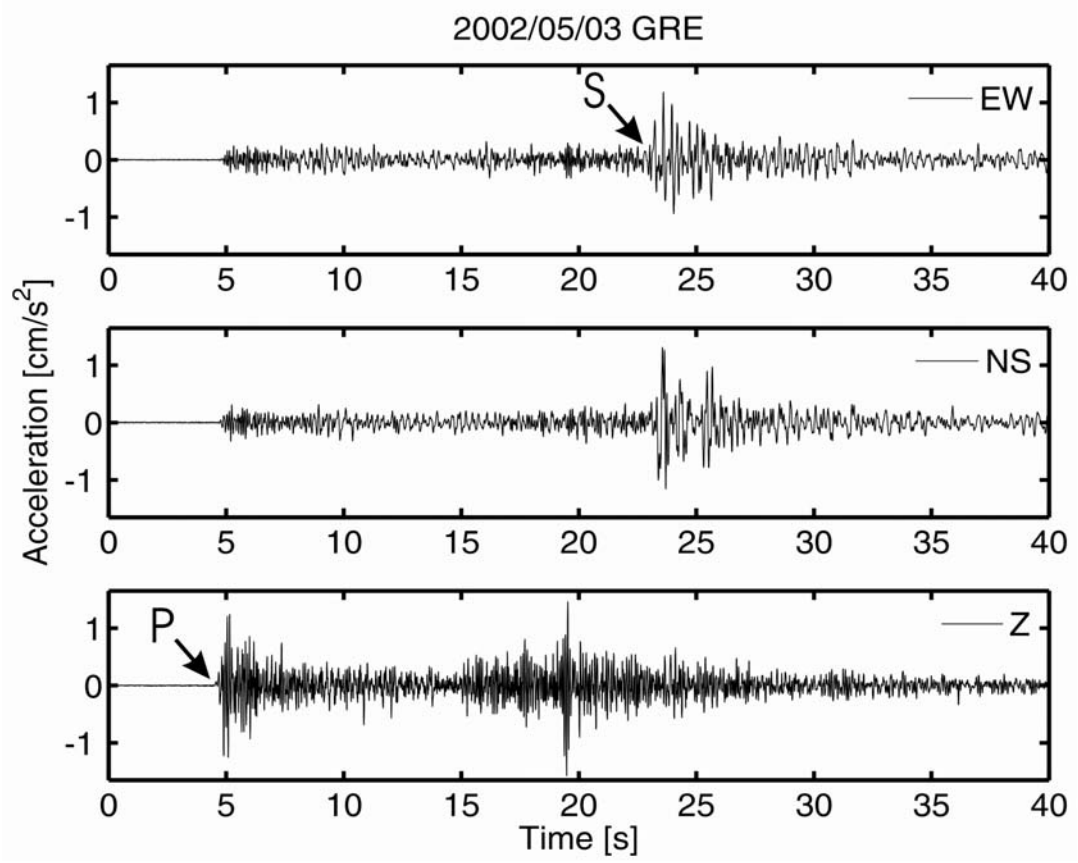

Figure 2. Example for the three-component recordings at station GRE. The accelerograms shown were obtained from a M_W=4.6 event in 162 km depth.

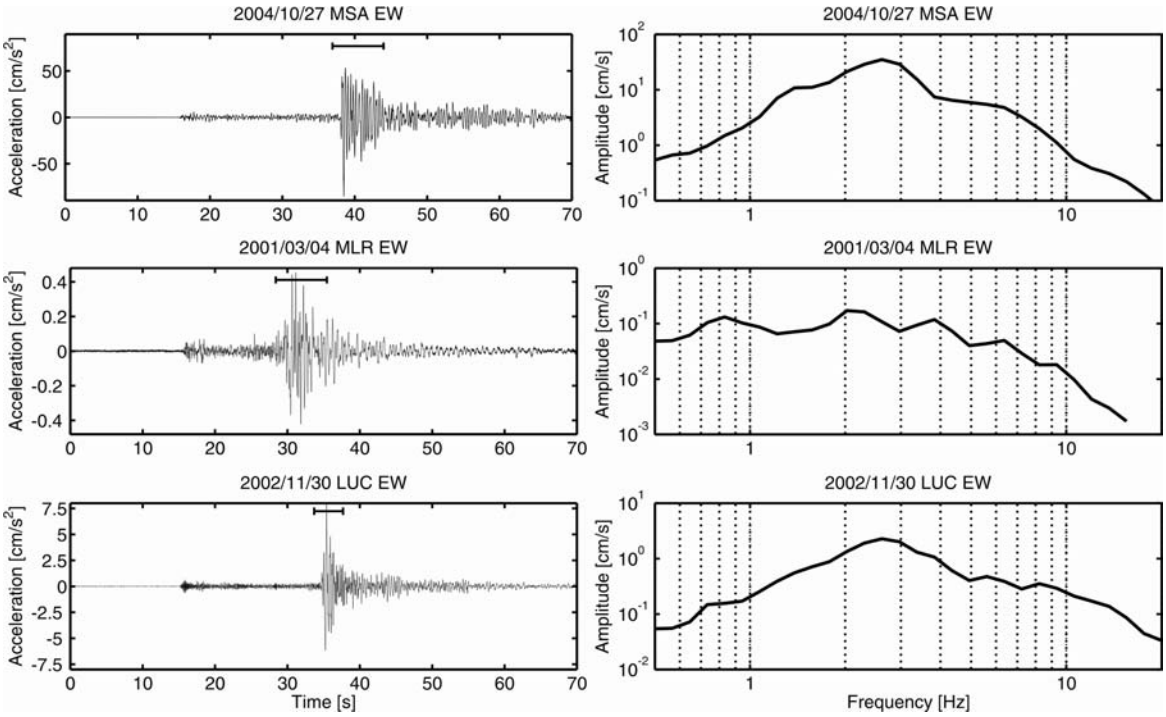

Figure 3. Left panel: Example records (EW components) and S-wave windows (marked by the bar above the time history) used for the computation of Fourier amplitude spectra. The origin of the time axis does not correspond to the origin time of the respective event, but has been adjusted for displaying purposes. Right panel: smoothed Fourier amplitude spectra of the selected S-wave windows.

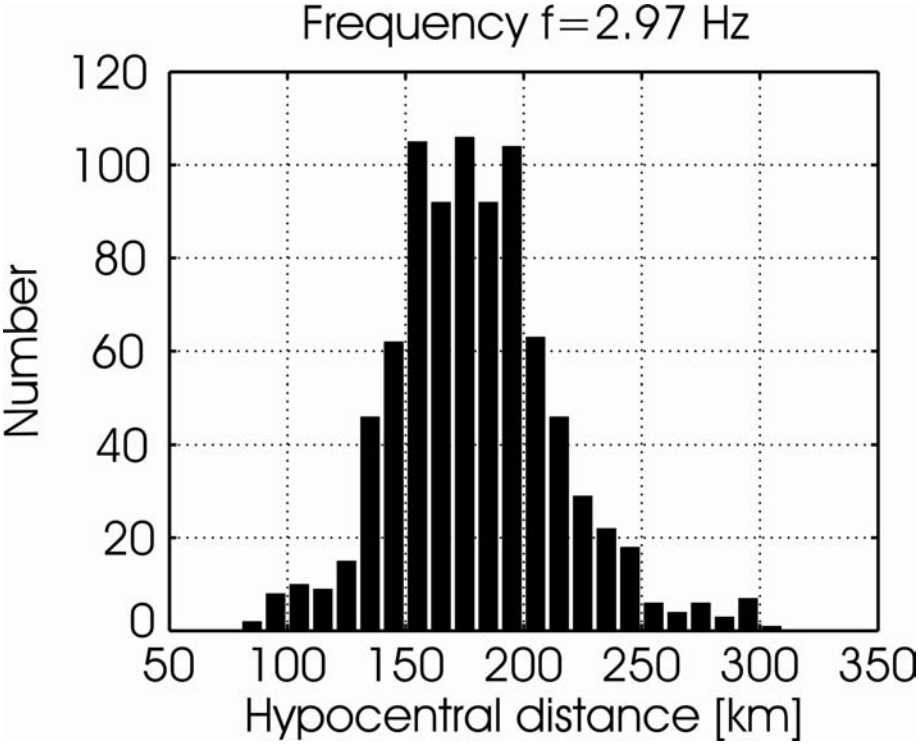

Figure 4. Example of the distribution of hypocentral distances in the dataset at one selected frequency. At lower frequencies, the database is slightly sparser due to signal-to-noise ratio constraints.

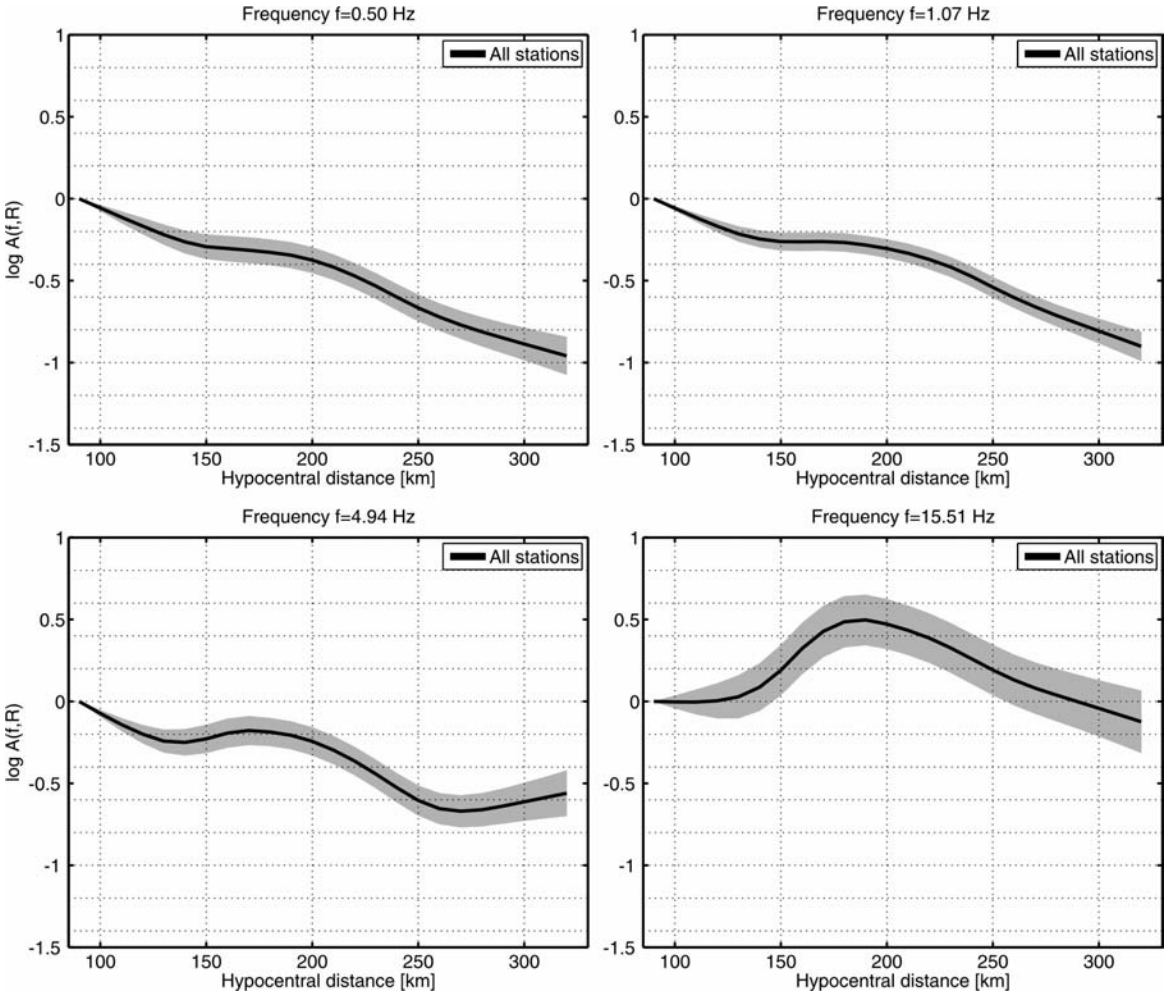

Figure 5. Attenuation functions (at four selected frequencies) obtained by fitting one function to the entire dataset at each frequency point. Black line: mean of 200 bootstrap samples. Grayshaded area: mean +/- one standard deviation.

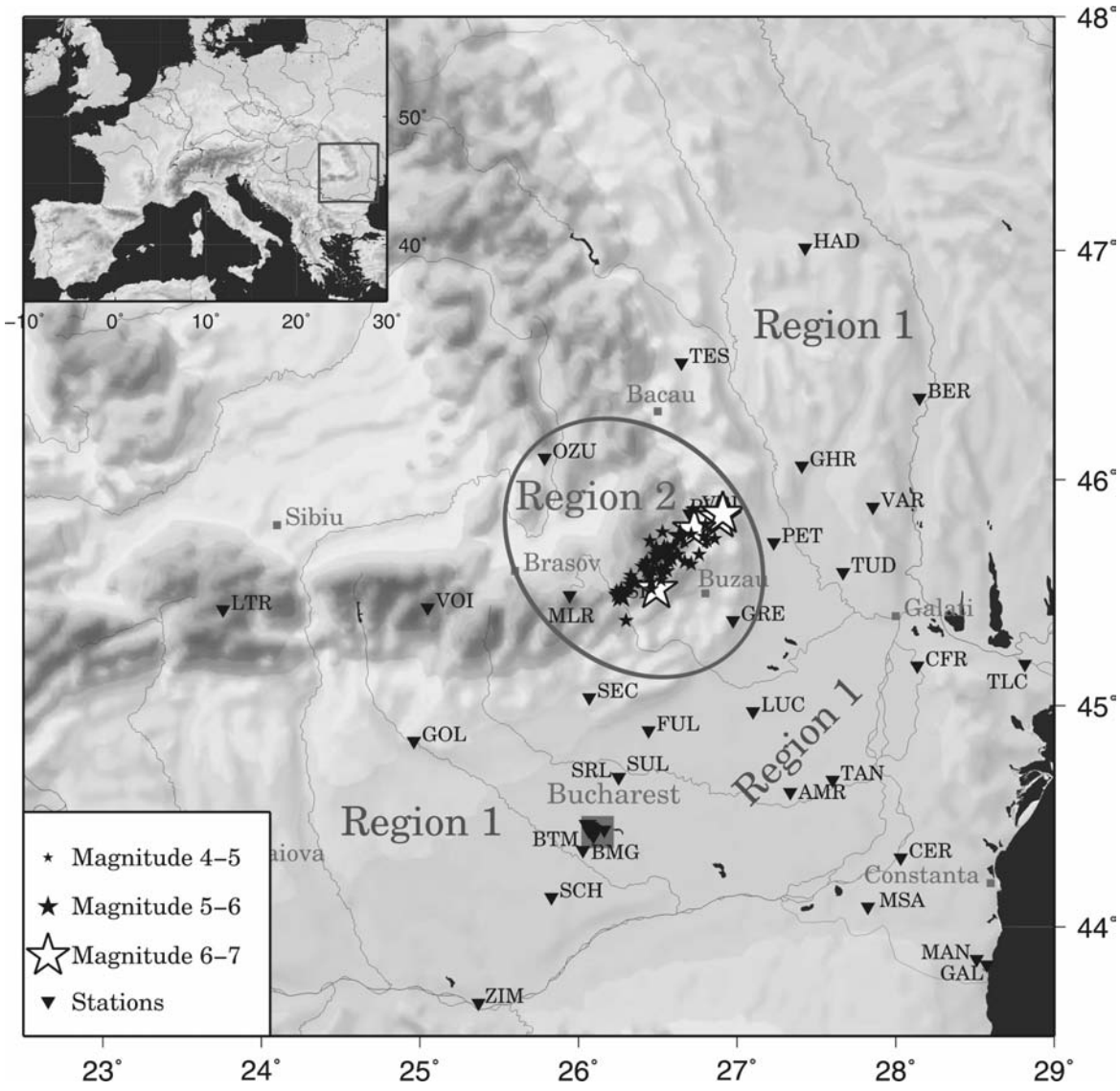

Figure 6. Map depicting the classification of the stations in region 1 and 2.

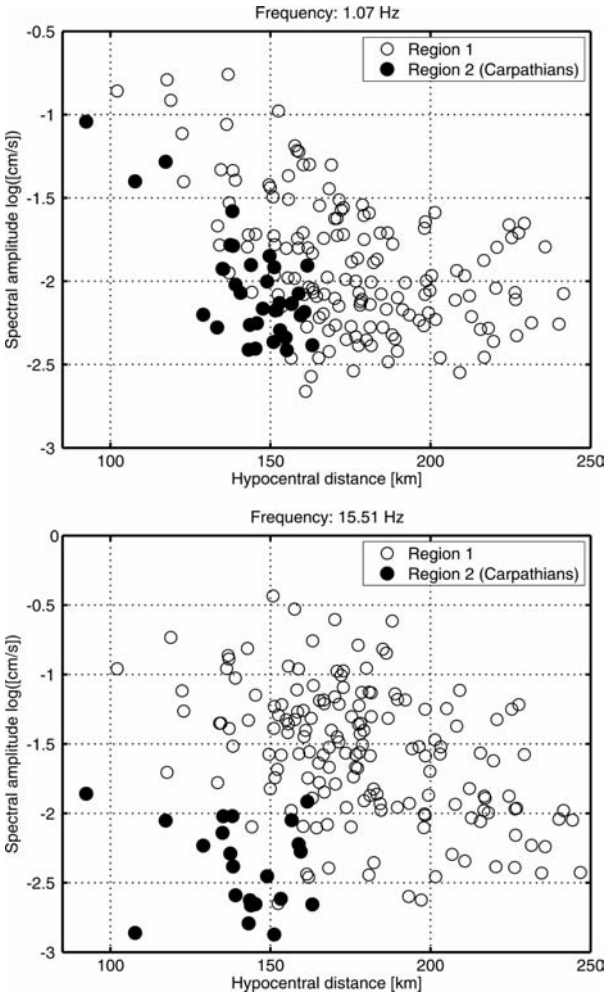

Figure 7. Spectral amplitudes observed at low frequencies (example at ≈ 1 Hz, top) and high frequencies (example at ≈ 15.5 Hz, bottom). Note that, with increasing frequency, the spectral amplitudes in region 2 get systematically lower than the ones in region 1 by up to one order of magnitude at similar distances.

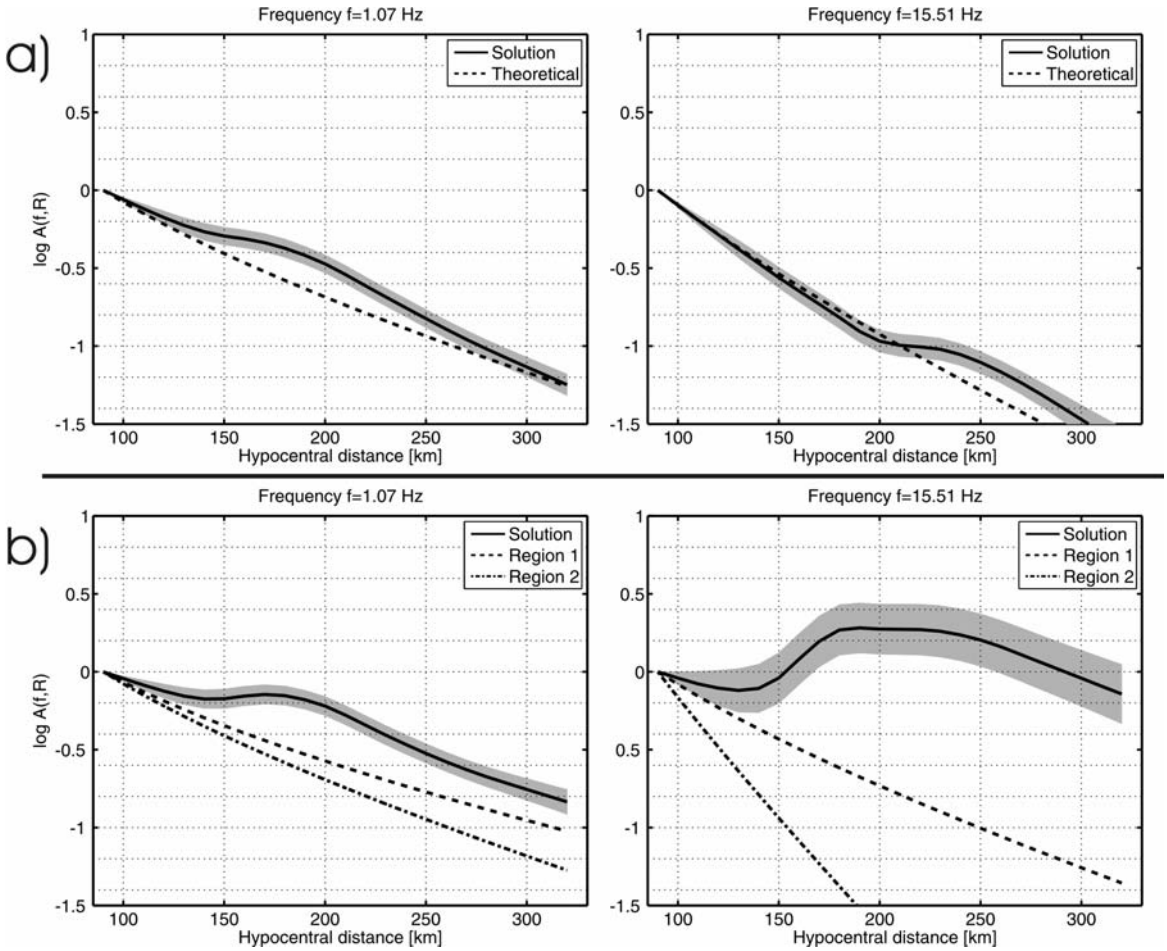

Figure 8. Attenuation functions derived from the synthetic data described in the text at two frequency points. Upper panel: *model A*. Lower panel: *model B*. The black line shows the mean of 200 bootstrap samples, while the grayshaded area delimits the region within one standard deviation. The theoretical models used in the computation of the synthetics are shown as dashed (*model A*) and dashed/dash-dotted lines (*model B*, for the two regions).

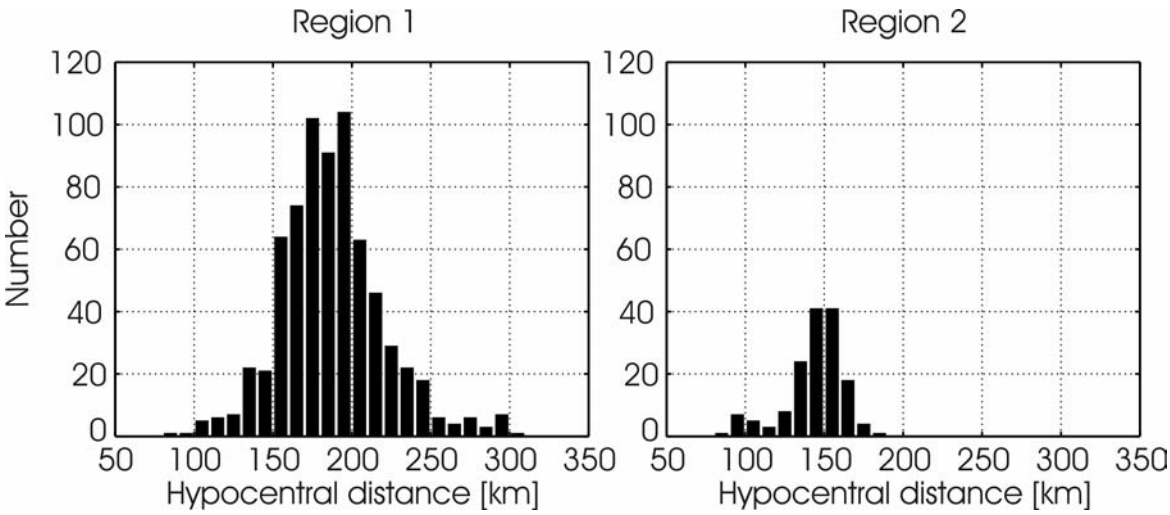

Figure 9. Example of the distribution of hypocentral distances in the dataset at one selected frequency (same as in Figure 4) separated in region 1 (left) and 2 (right).

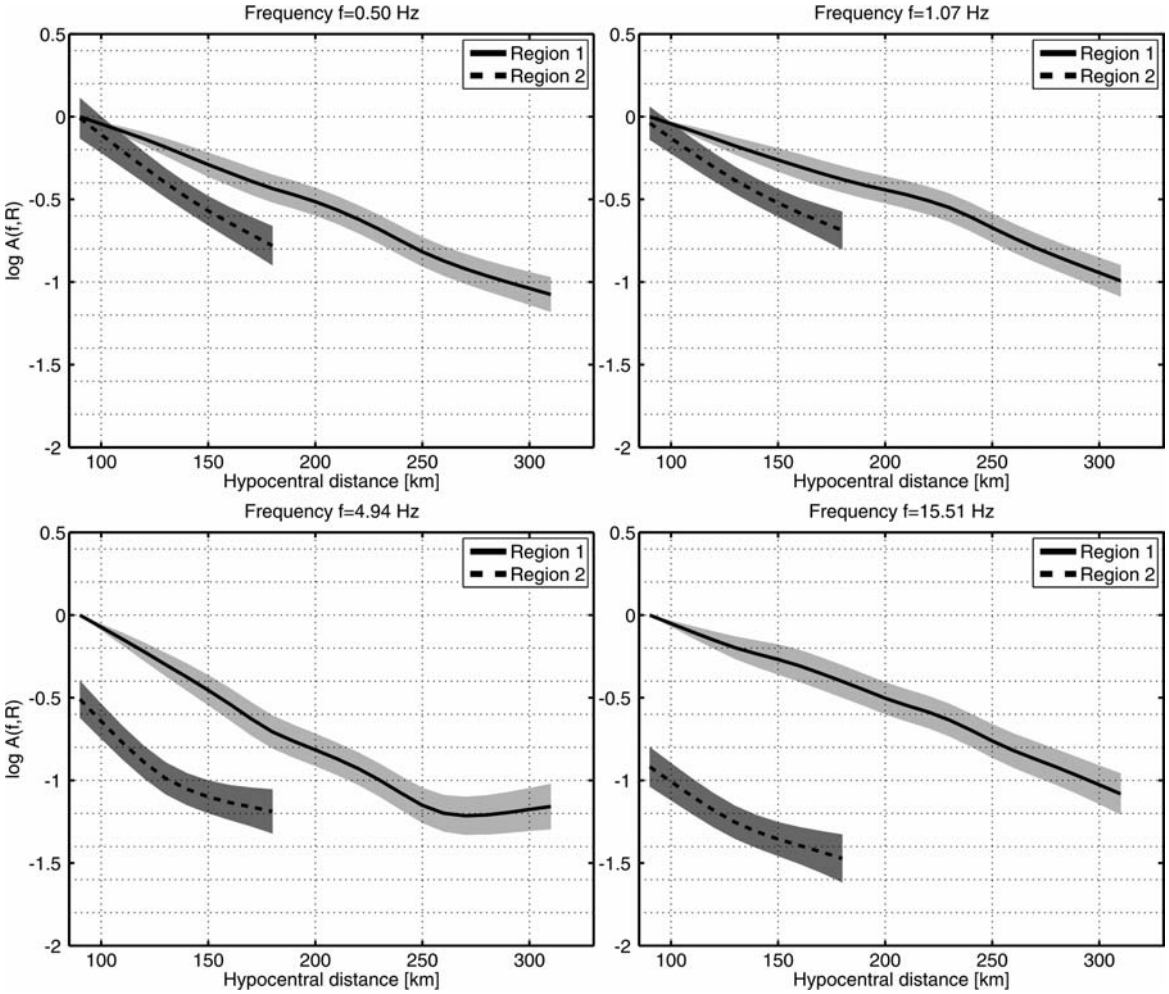

Figure 10. Attenuation functions (at four selected frequencies) obtained by fitting two separate functions for region 1 (continuous line) and 2 (dashed line) to the dataset at each frequency point using the modified inversion scheme. Grayshaded area: mean +/- one standard deviation.

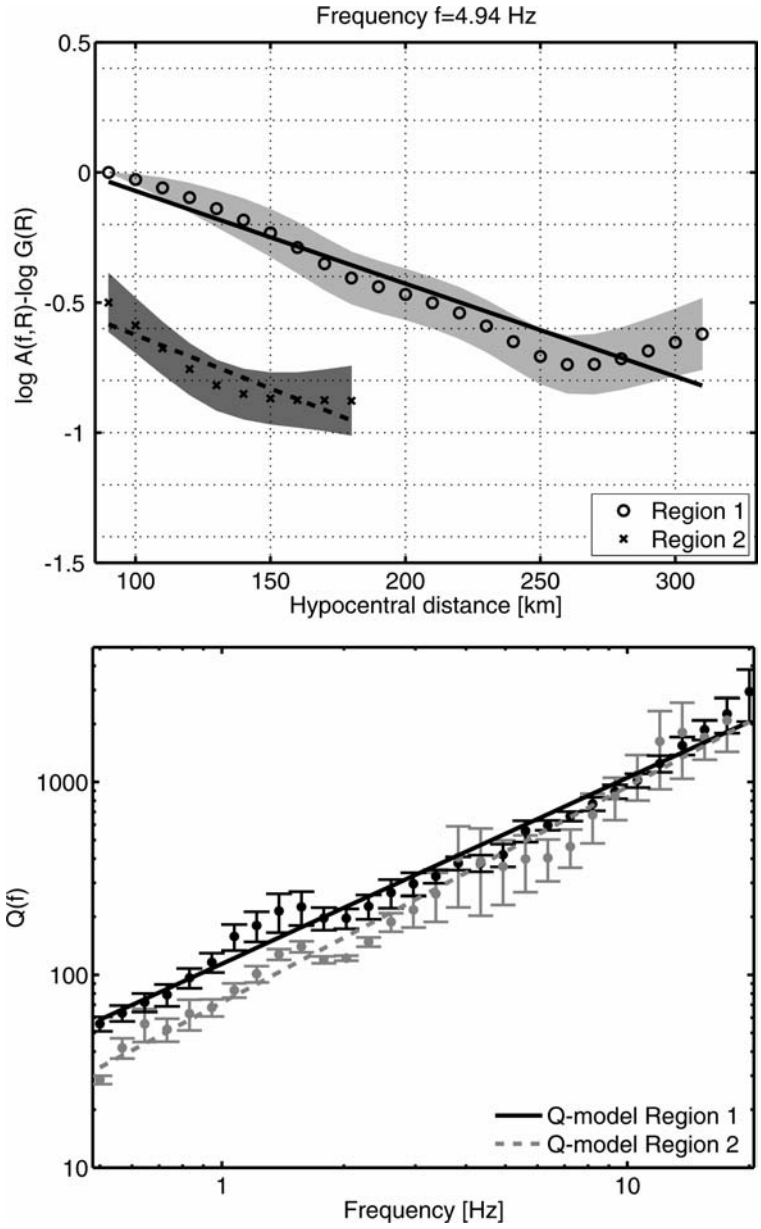

Figure 11. Top: Attenuation functions corrected for geometrical spreading ($\log A(f,r) - \log G(r)$ versus r) and fitted straight line (least squares fit) at one frequency point. Both functions (i.e. for region 1 and 2) are normalized to zero (in logarithm) at the reference distance r_0, but offset with 0.5 in the figure for displaying purposes. Bottom: Derived $Q(f)$-models for region 1 and 2 by evaluating the slope of the fitted lines at each frequency.

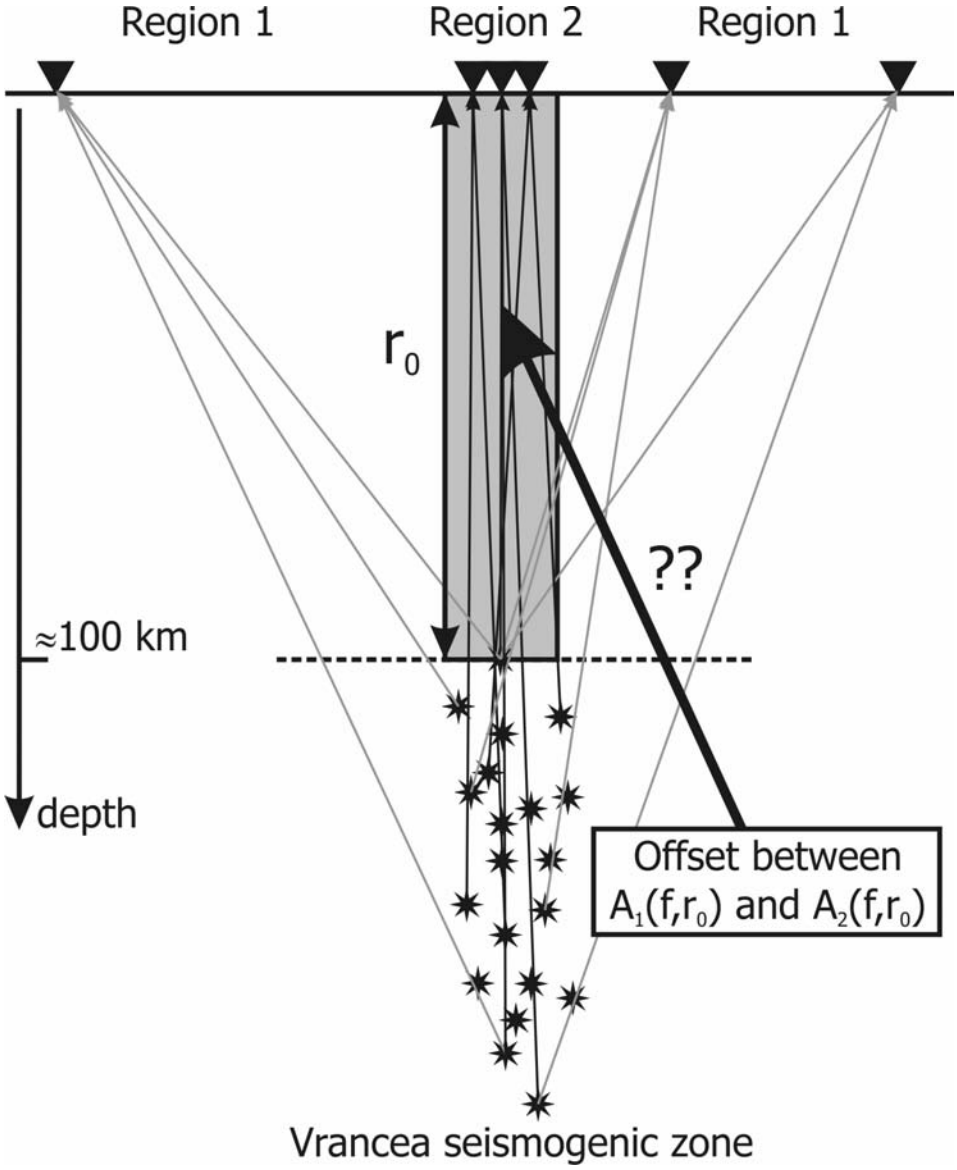

Figure 12. Sketch depicting the ray paths from sources to stations (orientation roughly SW-NE). For the stations in region 2, the rays from different earthquakes all travel the same path through the grayshaded region, which is defined by the depth of the shallowest event in the dataset. Increasing the distance *r* in the attenuation function $A_2(f,r)$ means to look mainly at data from deeper earthquakes and therefore, $A_2(f,r)$ only 'samples' the hypocentral zone. The offset between the origins of the two attenuation functions, $A_1(f,r_0)$ and $A_2(f,r_0)$, is related to a process occurring somewhere in the grayshaded zone.